Selective Oxidation of Glucose using Hydrogen Peroxide as an Oxidant

Reinsdorf, Ole; Pellegrin, Camille; Schmidt, Christoph; Alvear, Matias; Eränen, Kari; Murzin, Dmitry Yu; Salmi, Tapio

Published in:
ChemCatChem

DOI:
10.1002/cctc.202300536

Published: 01/08/2023

Document Version
Final published version

ChemCatChem

Research Article
doi.org/10.1002/cctc.202300536

Chemistry Europe
European Chemical Societies Publishing

www.chemcatchem.org

Selective Oxidation of Glucose using Hydrogen Peroxide as an Oxidant: On the Structure Sensitivity of the Apparent Activation Energy

Ole Reinsdorf,*[a] Camille Pellegrin,[a] Christoph Schmidt,[a] Matias Alvear,[a] Kari Eränen,[a] Dmitry Yu Murzin,[a] and Tapio Salmi[a]

The selective oxidation of glucose to gluconic acid with hydrogen peroxide was studied using different heterogeneous catalysts with alumina (Al_2O_3) and titanium silicate (TS-1, TiMWW) as supports and different noble (Au, Pd) and non-noble metals (Fe, W) as the catalytically active phases. Supported tungsten oxide catalysts showed a moderate selectivity and activity compared to palladium and iron catalysts. The best performance in the selective oxidation of glucose among the studied catalysts was displayed by gold on alumina. For this kind of catalyst, the structure sensitivity in glucose oxidation was explored, revealing a maximum rate shifted to larger gold particle sizes at higher temperatures in comparison with other studies involving activation of molecular oxygen on gold particles. A significant change in the apparent activation energy was established while changing the particle size of gold. These changes of the activation energy were adequately explained by a theoretical model for the cluster size dependence of the apparent activation energy.

Introduction

In the recent years the development of sustainable alternatives for conventional reaction routes has been taken the spotlight in chemical research. Especially the valorisation of biomass has attracted a lot of attention. Transformation of sugars originating from lignocellulosic biomass into value- added products, such as sugar acids and sugar alcohols with various catalytic processes is a part of these efforts.[1–2] These aldonic acids (sugar acids) are used in pharmaceutical, cosmetic, alimentary and detergent industries due to their excellent properties of biodegradability and biocompatibility.[2–5] The oxidation of monosaccharides usually carried out in the presence of either noble metal catalysts or enzymes with molecular oxygen as the oxidizing agent. Particularly gold and palladium have been used as active metals for this reaction. The focus in the recent years has laid on catalytic gold due to its better stability and performance compared to palladium.[5–11] Other noble metals like platinum, which is known to catalyze C–H bond activation,[12–14] play a less important role in recent years. However, are of high interest in the electrocatalytic reaction.[15] Hydrogen peroxide formed via an oxygen reduction mechanism has been proposed as a surface intermediate in the oxidation process, while hydrogen peroxide as an oxidant has been applied in few studies with gold catalysts. The scopes of the previous studies have been rather limited, focusing primarily on the catalyst support and parameter optimization.[16–23] This parameter optimization revealed mild basic conditions, a minor excess of hydrogen peroxide and a moderate temperature range 70 to 90 °C as optimal conditions.[17] Additionally several methods of process intensifications have been employed. Omri et al.[19] and Rautianen et al.[21] demonstrated that microwave irradiation can substantially enhance the reaction performance. A similar increase in the reaction rates was achieved through photo-irradiation by Omri et al.[18] In all these studies Au/Al_2O_3 was the most applied system while other supports have been employed to a lesser extent. Mechanistically the system involves the formation of a hydroperoxide species formed on the catalyst, which reacts with the hydrate form of glucose formed under basic conditions on the catalyst surface.[19] The benefit of using hydrogen peroxide instead of oxygen is that higher concentrations of the oxidant become possible, not being limited by gas solubility. Besides the interest for the production of gluconic acid the reaction is used for electrochemical sensors for glucose.[24,26] In this work, selective oxidation of glucose, as a model molecule, with different catalytic metals and supports, as well as nanoparticle particle sizes has been investigated. Besides screening suitable catalysts for glucose oxidation, structure dependence of the activation energy of the sugar oxidation with hydrogen peroxide is for the first time reported.

Results and Discussion

Catalyst characterization. All nanoparticle sizes were determined with TEM with the results summarized in Figures 1–12. For gold catalysts with higher particle sizes exceeding 20 nm,

[a] O. Reinsdorf, C. Pellegrin, C. Schmidt, M. Alvear, K. Eränen, D. Y. Murzin, Prof. T. Salmi
Laboratory of Industrial Chemistry and Reaction Engineering (TKR)
Åbo Akademi University Turku
FI-20500 Turku/Åbo (Finland)
E-mail: ole.reinsdorf@abo.fi

Supporting information for this article is available on the WWW under https://doi.org/10.1002/cctc.202300536

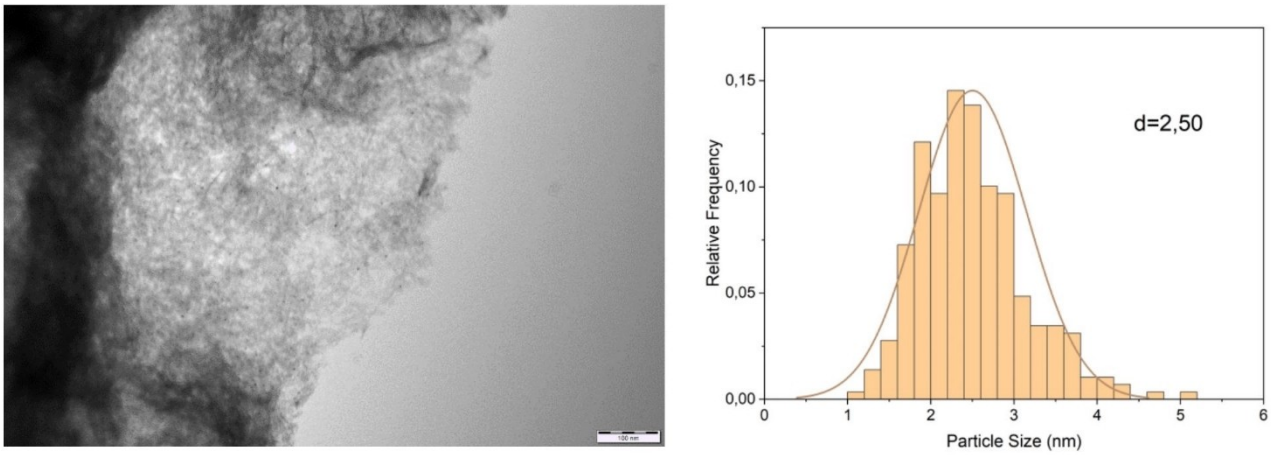

Figure 1. Transmission electron micrograph and the corresponding histograms for the catalyst 2 wt% Au/Al_2O_3_ 2.5 nm.

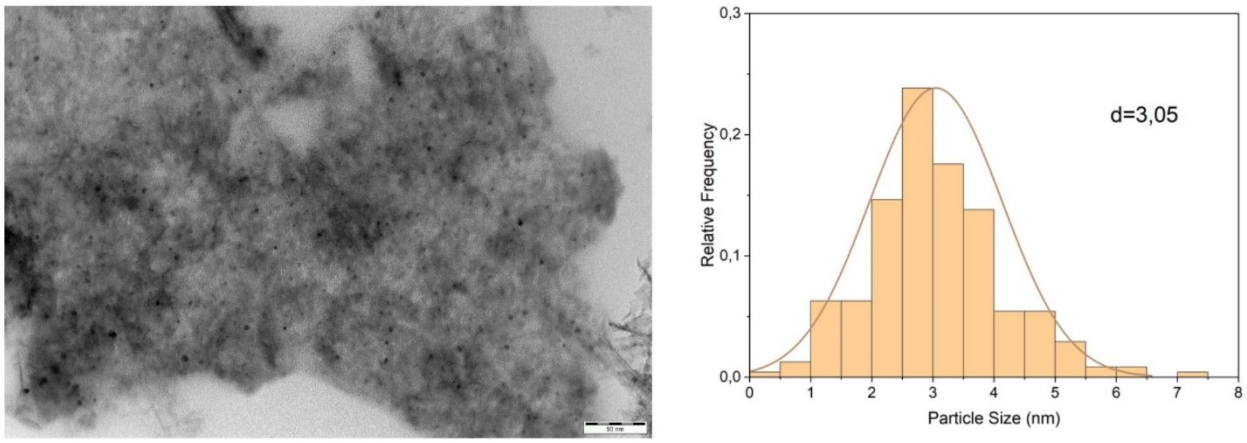

Figure 2. Transmission electron micrograph and the corresponding histograms for the catalyst 2 wt% Au/Al_2O_3_ 3 nm.

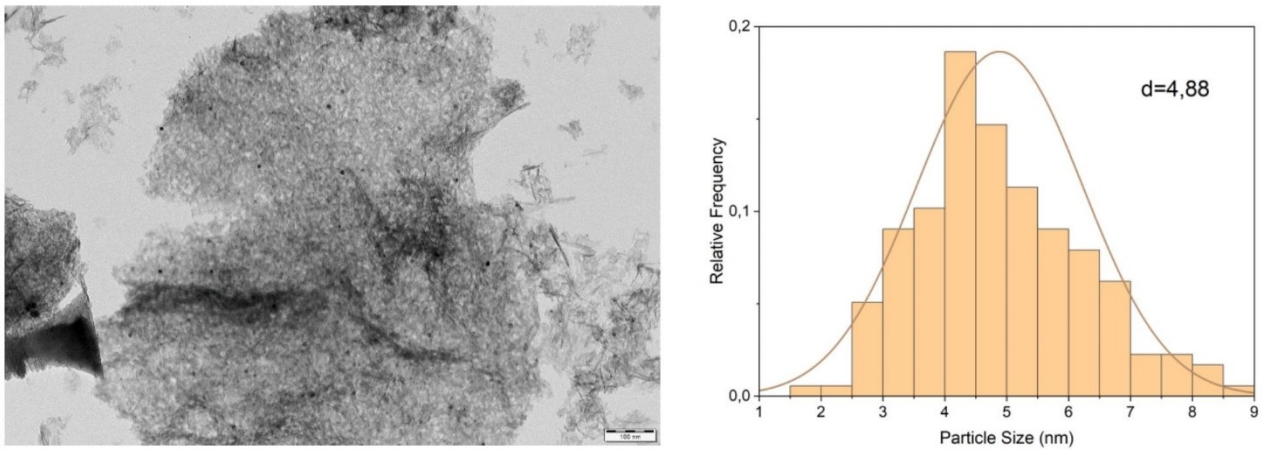

Figure 3. Transmission electron micrograph and the corresponding histograms for the catalyst 2 wt% Au/Al_2O_3_ 4.88 nm.

bigger conglomerates of smaller particles were observed. However, gold catalysts with the average cluster below 7.1 nm exhibited good uniformity of all particles. The synthesized palladium catalyst showed, besides smaller dispersed particles, spots of a higher density of those particles.

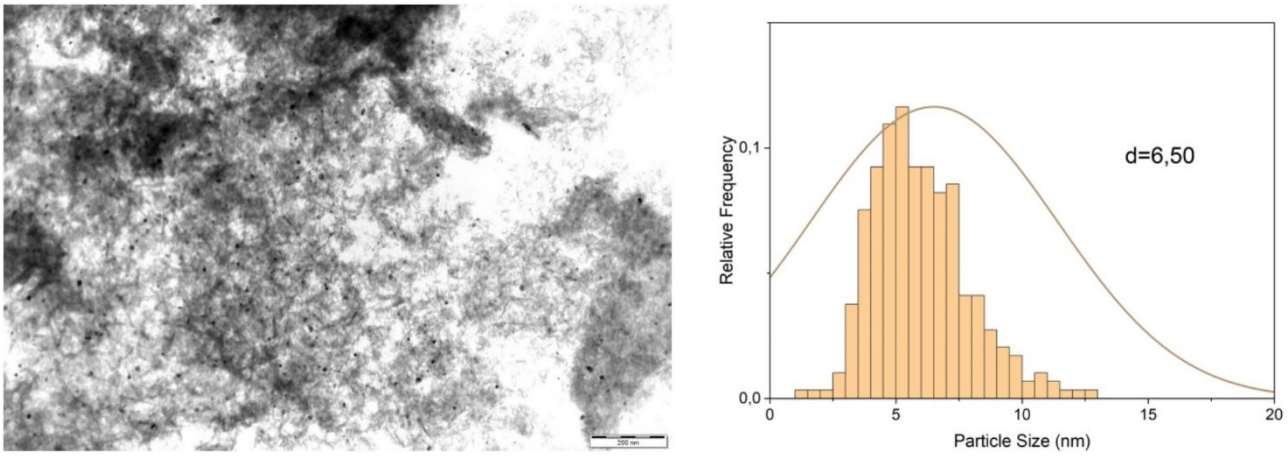

Figure 4. Transmission electron micrograph and the corresponding histograms for the catalyst 2 wt% Au/Al_2O_3_ 6.5 nm.

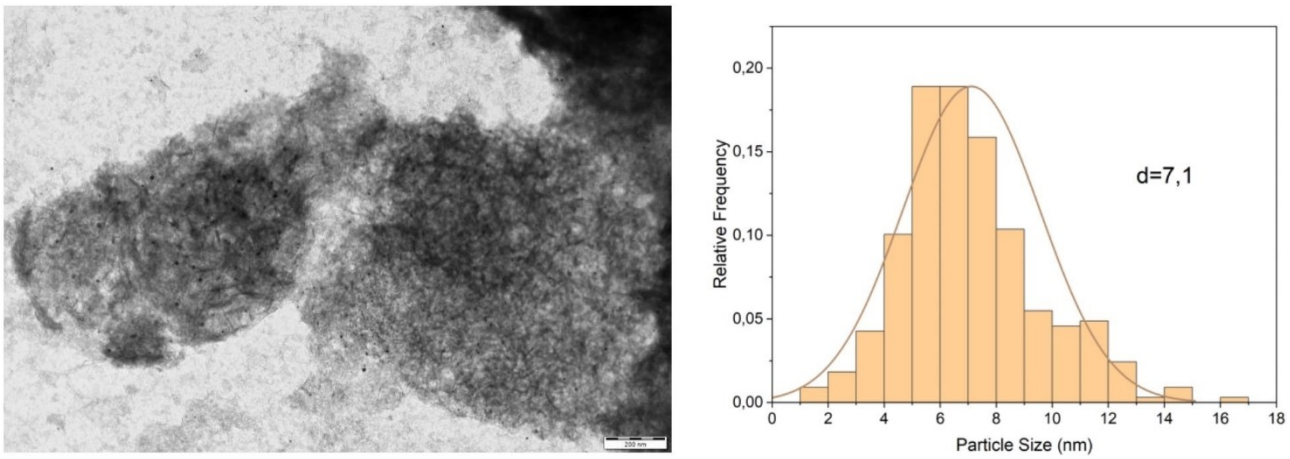

Figure 5. Transmission electron micrograph and the corresponding histograms for the catalyst 2 wt% Au/Al_2O_3_ 7 nm.

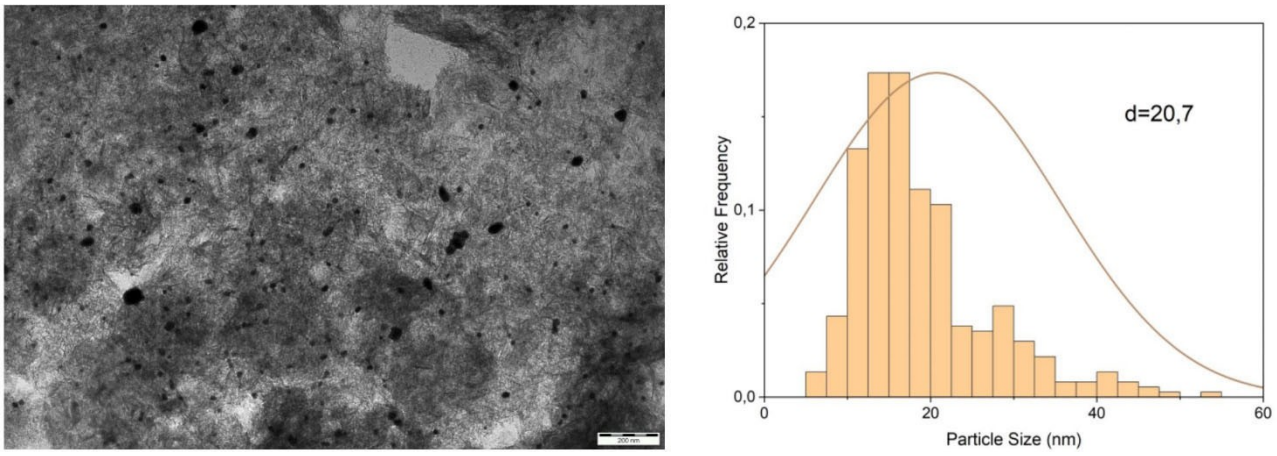

Figure 6. Transmission electron micrographs and the corresponding histograms for the catalysts 2 wt% Au/Al_2O_3_ 20.7 nm.

Changes in the synthesis method and calcination temperature did not lead to any significant changes in acidity, surface area or the pore size of the alumina support. Subsequently it can be concluded that the impact of the support properties on

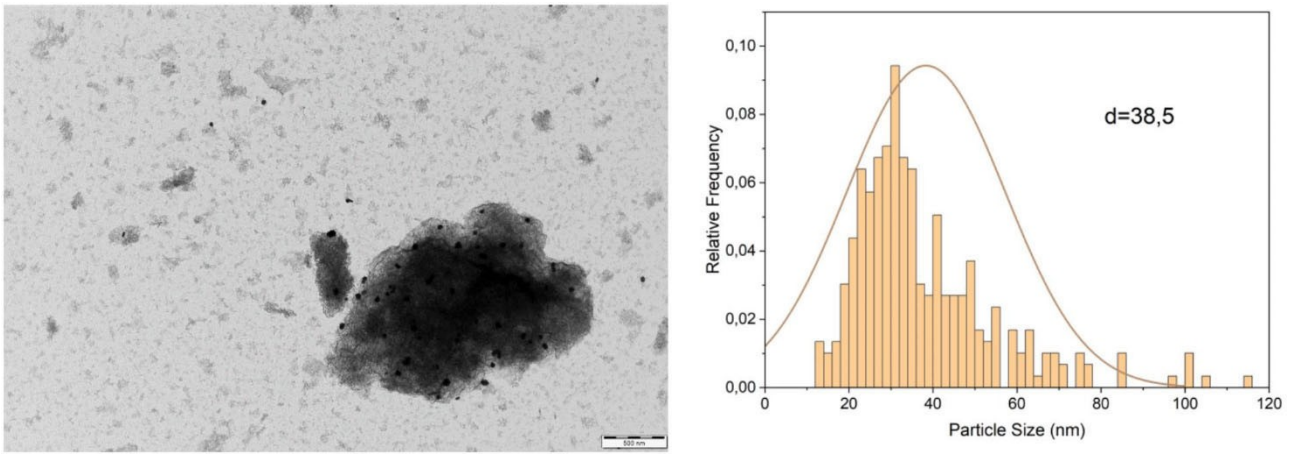

Figure 7. Transmission electron micrographs and the corresponding histograms for the 2 wt% Au/Al_2O_3_ 38 nm.

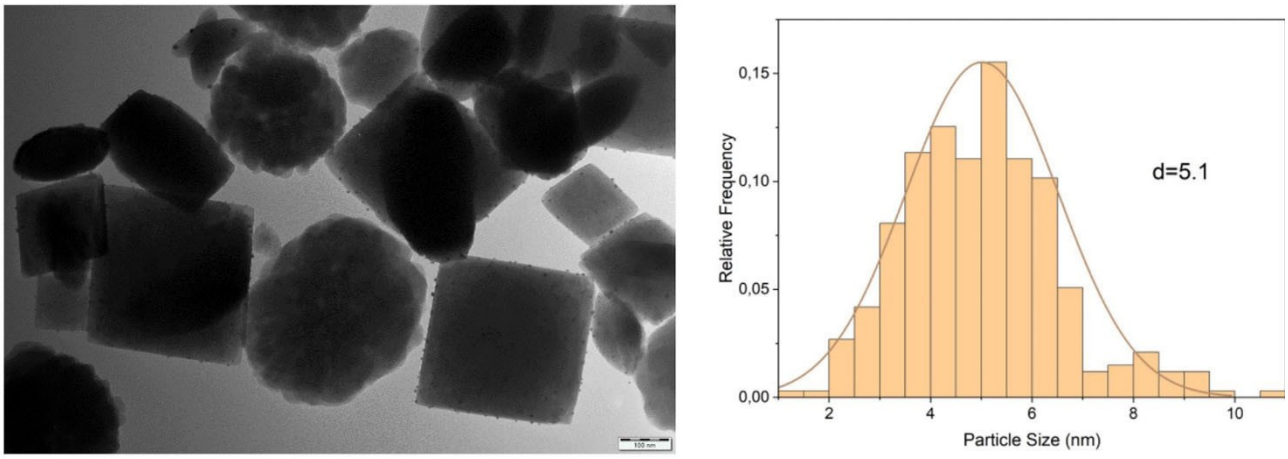

Figure 8. Transmission electron micrographs and the corresponding histograms for the catalysts 2 wt% Au/TS-1.

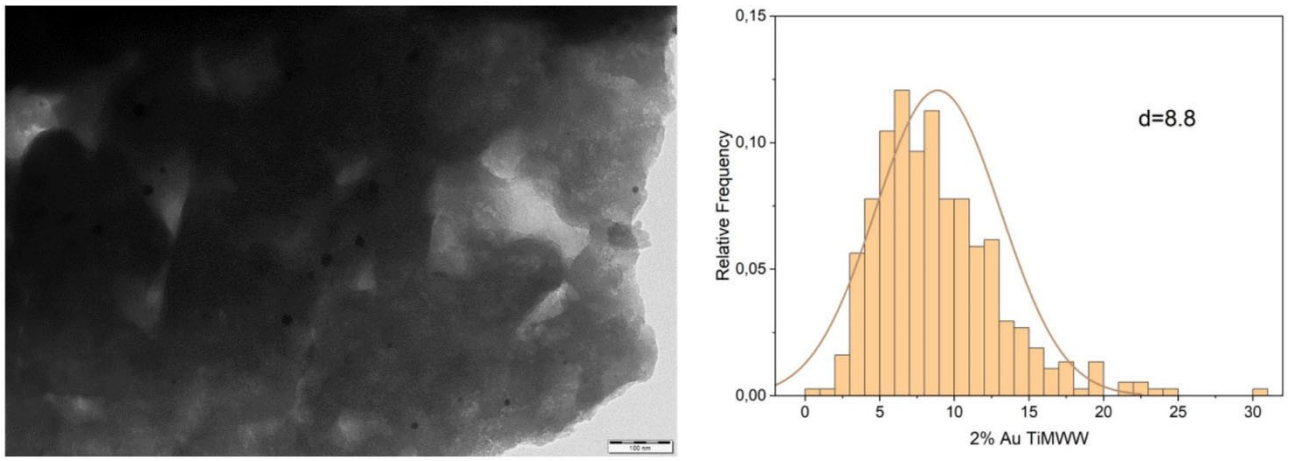

Figure 9. Transmission electron micrographs and the corresponding histograms for the catalysts 2 wt% Au/TiMWW.

the catalytic performance is negligible. The characterization results are summarized in Table 1.

Blank experiments. Blank experiments were conducted for the mixture of a hydrogen peroxide and a sugar solution with

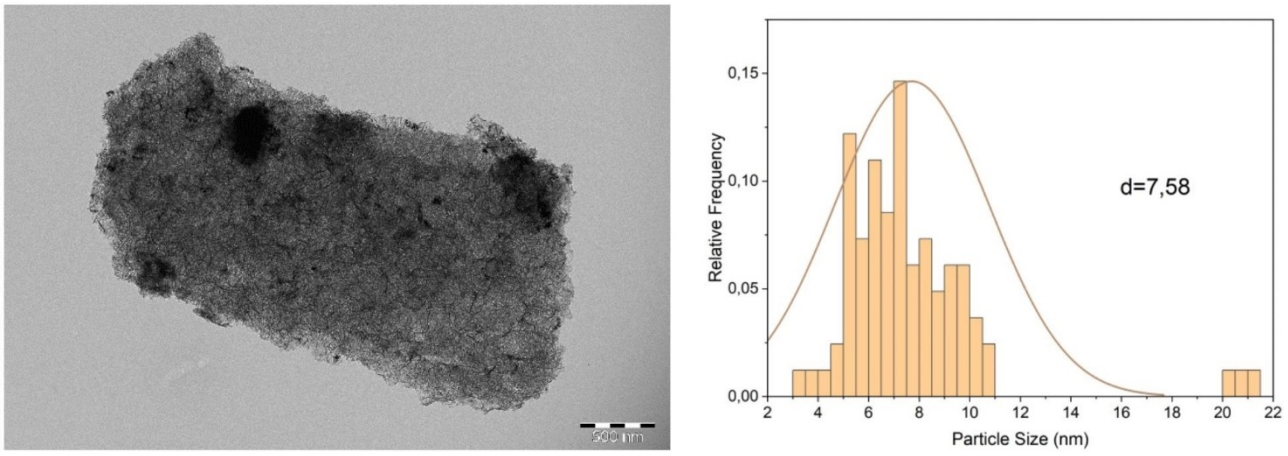

Figure 10. Transmission electron micrograph and the corresponding histograms for the catalyst 1 wt% Pd/Al_2O_3.

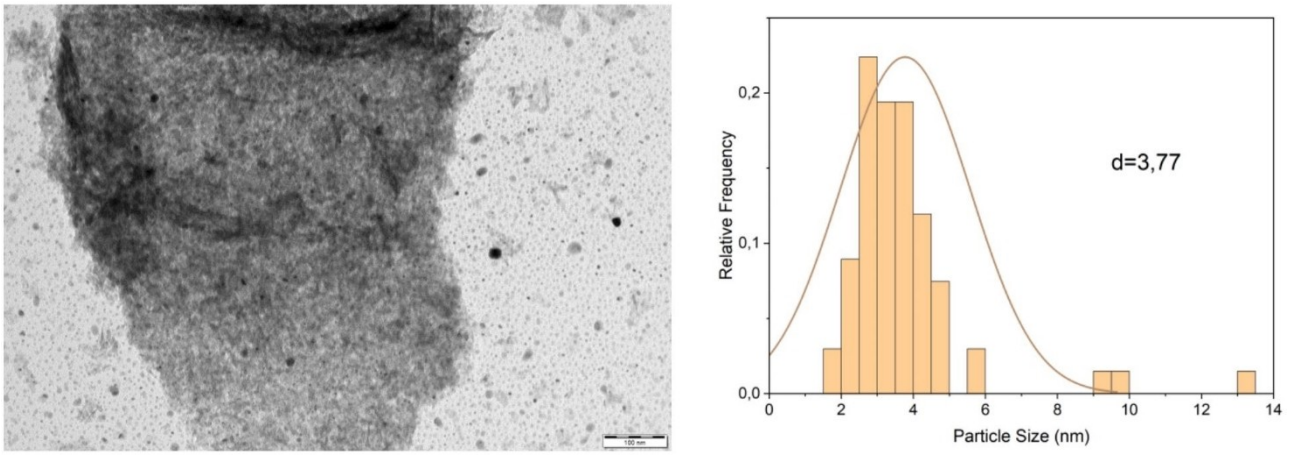

Figure 11. Transmission electron micrograph and the corresponding histograms for the catalyst 2 wt% Fe/Al_2O_3.

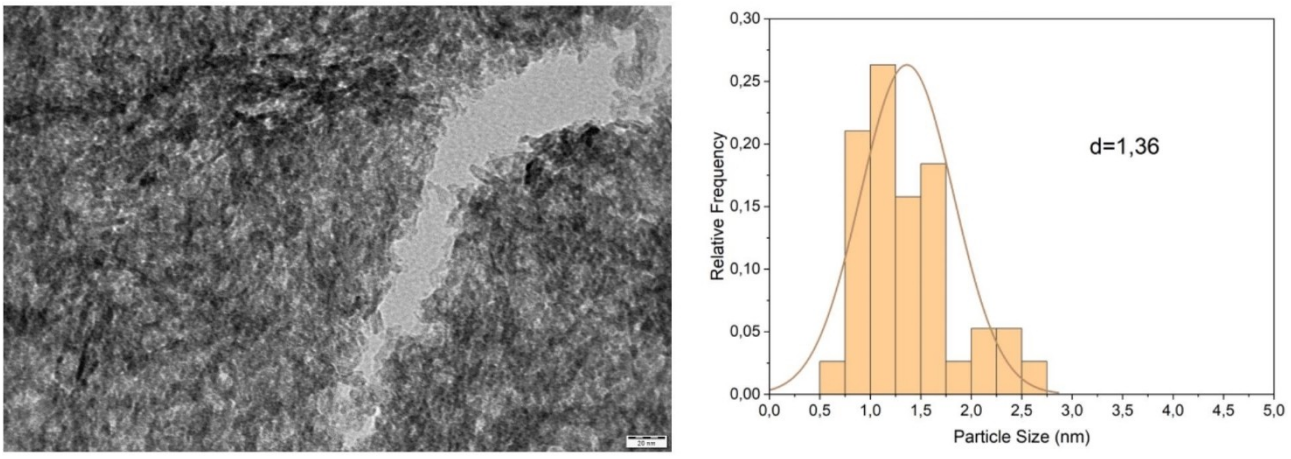

Figure 12. Transmission electron micrograph and the corresponding histograms for the catalyst 2 wt% W/Al_2O_3.

unmodified supports and without any additives. The oxidation reactions performed in the absence of gold displayed for all blank experiments a very low or non-existing selectivity to gluconic acid. However, formation of formic acid was observed,

Table 1. Synthesis method and properties of the synthesised catalysts.

Catalyst	Synthesis method	Nanoparticle size [nm]	Metal loading [%]	Surface area [m^2/g]	d_{pore} [nm]	$c_{LewisAcid}$ [mmol/g]
2 wt% Au/Al_2O_3_2.5	DP	2.50	1.82	210	9.8	0.063
2 wt% Au/Al_2O_3_3	DP	3.01	1.70	188	9.7	0.056
2 wt% Au/Al_2O_3_4.88	DP	4.88	1.92	200	11.0	0.056
2 wt% Au/Al_2O_3_6.5	DP	6.50	1.90	210	10.	0.058
2 wt% Au/Al_2O_3_7	DP	7.10	1.93	196	11.1	0.056
2 wt% Au/Al_2O_3_20	DP	20.7	1.92	226	10.	0.058
2 wt% Au/Al_2O_3_38	EI	38.5	2.15	220	10.6	0.058
2 wt% Au/TS1	DP	5.11	2.25	240	7.5	0.573
2 wt% Au/TiMWW	DP	8.82	2.05	489	22.1	1.182
1 wt% Pd/Al_2O_3	EI	7.58	1.09	220	9.9	0.043
2 wt% Fe/Al_2O_3	IWI	3.73	2.31	167	11.2	0.053
2 wt% W/Al_2O_3	IWI	1.14	1.98	207	10.9	0.047

being mainly attributed to C–C scission. Such a formation of formic acid is starting slowly at the beginning of an experiment but accelerating substantially eventually slowing down after reaching a concentration limit, a profound S-curve is obtained as depicted in Figure 13.

The strong S-shape of concentration curve typically indicates an autocatalytic behaviour. A plausible explanation for such behaviour is related to formation of performic acid due to presence of formic acid and hydrogen peroxide in the reaction medium.[27] Subsequently performic acid can accelerate further C–C scission leading to the S-shaped concentration curves. However, this behaviour slows down with a decreasing hydrogen peroxide concentration, which is apparently related to slower performic acid formation. Slower rates were detected on titanium silicates, indicating a strong dependency of formation of the peracid on the type of the peroxide species formed by the support. Levulinic acid, a product of the glucose splitting formed in stoichiometric quantities with formic acid, was detected in the experiments, too. Both reactants were formed in a ratio of $\frac{C(Formic\ Acid)}{C(Levulinic\ Acid)} = 1.06$.

Experiments using only hydrogen peroxide and the supports revealed no significant peroxide decomposition during the reaction time. In the absence of catalysts and supports, no reactions were observed as expected.

Role of the support. Three different supports were screened, namely alumina and two titanium silicates. The latter are well known to catalyse various oxidation reactions with hydrogen peroxide.[28–30] All the catalysts showed a considerable oxidation activity. However, both titanium silicates displayed a lower overall rate giving a lower overall conversion after two hours as illustrated in Figure 14, which apparently reflects catalyst deactivation because the oxidation reaction is not limited by thermodynamics.

The alumina-supported catalyst exhibited the best performance reaching a complete glucose conversion after 50 minutes. Both alumina and TS1 as supports for gold afforded an excellent selectivity exceeding 95 %, while for TiMWW 84 % was obtained giving gluconic, glucaric and trace amounts of formic and levulinic acids. The results are summarized in Table 2.

Role of metal. Gold and palladium were selected as catalytic metals due to their well-known activity and selectivity in the oxidation of glucose reported in previous studies, whereas iron and tungsten were chosen due to their ability to activate hydrogen peroxide.[31–36] In the experiments, gold exhibited the highest activity and selectivity, in a steep contrast to palladium and iron which promoted the C–C scission and formed

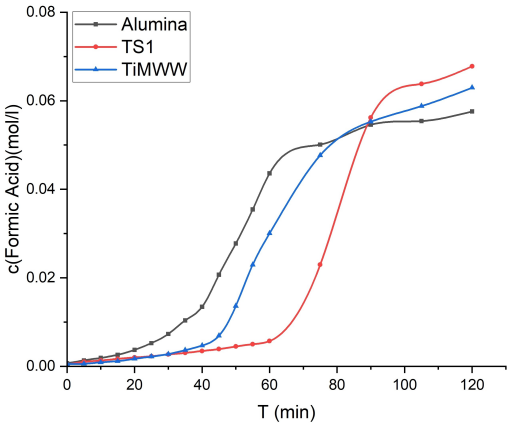

Figure 13. Evolution of the formic acid concentration on the supports in the absence of gold ($\vartheta = 70\,^{\circ}C$, c(Glucose) = 0.2 M, $c(H_2O_2) = 1.5$ M, $m_{cat} = 100$ mg).

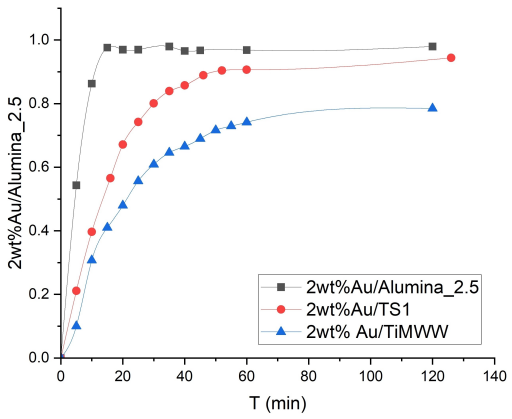

Figure 14. Yield of gluconic acid on different supported gold catalysts ($\vartheta = 70\,^{\circ}C$, c(Glucose) = 0.2 M, $c(H_2O_2) = 1.5$ M, mcat = 100 mg).

Table 2. Results of the catalyst screening experiments with different supports. (T = 70 °C, pH = 8, c(Glucose) = 0.2 M, $c(H_2O_2)$ = 1.5 M).

Catalyst	Initial oxidation rate [mol/(g_{metal} min)]	Conversion (2 h) [%]	Selectivity (GlcAc) [%]
2% Au/Al_2O_3_2.5 nm	1.22	99.1	97.5
2% Au/TS-1	0.94	98.8	95.4
2% Au/TiMWW	0.83	93.1	84.2

predominantly formic acid. The tungsten oxide catalyst however, retained a moderate selectivity over the longer reaction times after a high initial selectivity. The results are depicted in Figure 15 and Table 3. Subsequently, the gold catalysts were selected to further explore structure sensitivity.

Structure sensitivity. To study the structure sensitivity of the reaction on gold, seven gold catalysts with varying nanoparticle sizes between 2.5 nm and 38 nm were prepared. The performance of these catalysts was tested at the same conditions as described before. In addition, five selected catalysts were studied at 30 °C and 90 °C to reveal the structure sensitivity of the apparent activation energy of the reaction. This aspect of the structure sensitivity is seldom studied in the literature but it can provide a deeper insight in the reaction kinetics. No leaching of gold was observed in these experiments.

The results obtained at 70 °C are depicted in Figure 16. The rate shows a maximum at gold nanoparticle sizes of about 6 to 7 nm, which is significantly higher than the particle size used previously for the oxidation of glucose with hydrogen peroxide.[19,37] Taking into account the metal dispersion, the turnover frequency (TOF) was calculated according to Equation (1):

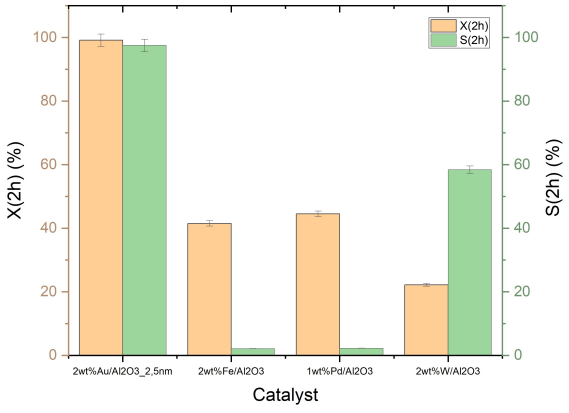

Figure 15. Influence of the metal on glucose oxidation with hydrogen peroxide (ϑ = 70 °C, c(Glucose) = 0.2 M, $c(H_2O_2)$ = 1.5 M, m_{cat} = 100 mg).

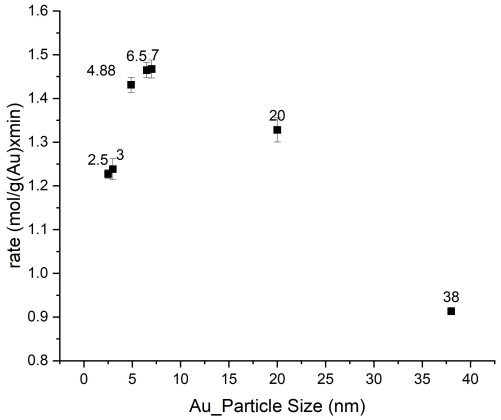

Figure 16. Particle size dependence of the reaction rate to gluconic acid of the gold catalysts at 70 °C.

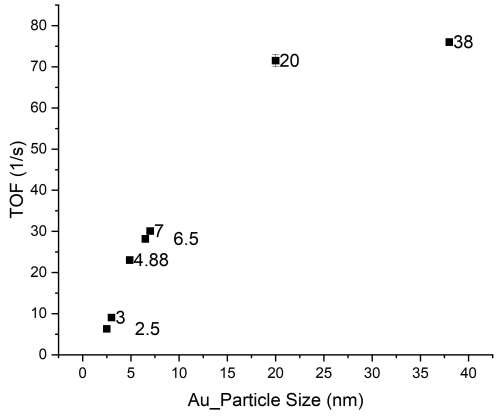

Figure 17. Particle size dependence of the TOF of the gold catalysts at 70 °C.

$$TOF = \frac{n(Glucose)^{*}X}{n(Au)^{*}D(Au)^{*}t} \quad (1)$$

based on the rates determined at t = 10 min, with X as the conversion of Glucose and D as the dispersion of gold.

A steady increase of TOF with an increase of the particle size was observed, but essentially levelling off beyond a particle size of 20 nm as visible from Figure 17.

At a lower temperature (30 °C), however, only a decrease of the rate as a function of the cluster size was visible (Figure 18), resulting in a much flatter profile of TOF vs the particle size (Figure 19).

On the contrary, upon an increase of the reaction temperature from 70 to 90 °C even a broader maximum in the rate vs

Table 3. Results of the catalyst screening experiments. (T = 70 °C, pH = 8, c(Glucose) = 0.2 M, $c(H_2O_2)$ = 1.5 M).

Catalyst	Initial oxidation rate [mol/(g_{metal} min)]	Conversion (2 h) [%]	Selectivity (GlcAc) [%]
2% Fe/Al_2O_3	0.16	41.5	2.13
1.5% Pd/Al_2O_3	0.37	44.5	2.25
2% W/ Al_2O_3	0.04	22.2	58.4

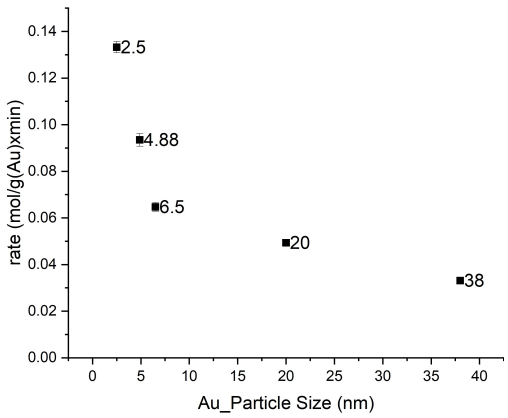

Figure 18. Particle size dependence of the reaction rate to gluconic acid of the gold catalysts at 30 °C.

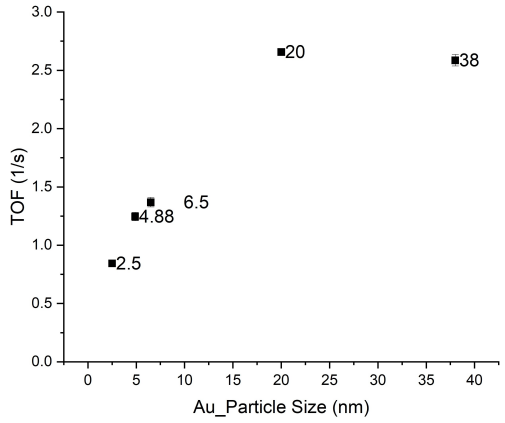

Figure 19. Particle size dependence of the TOF of the gold catalysts at 30 °C.

the particle size was observed as depicted in Figures 20 and 21. Based on the rates determined at the different temperatures, the apparent activation energies were estimated for different nanoparticle sizes. Comparing the resulting apparent activation

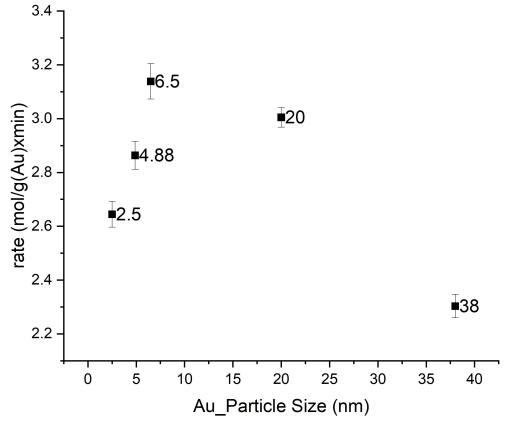

Figure 20. Particle size dependence of the reaction rate to gluconic acid of the gold catalysts at 90 °C.

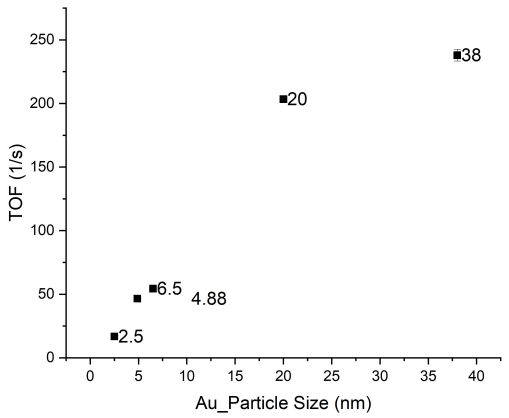

Figure 21. Particle size dependence of the TOF of the gold catalysts at 90 °C.

energies, an increase in the activation energy for bigger gold particle sizes was observed, following a stepwise increase of the apparent activation energy between particle sizes 2.5 and 6.5 nm and a plateau after 20 nm as displayed in Figure 22

The value obtained for the average particle size 2.5 nm of ca. 46 kJ/mol is in a good agreement with the activation energies reported in the literature for d-glucose oxidation with hydrogen peroxide in the presence of gold particles in the range of ca. 2 nm.[17] The differences in the apparent activation did not lead to changes in the selectivity to gluconic acid as depicted in Figure 23. Only for particle sizes of 30 nm a decrease in selectivity is observed. However, this decrease is more likely based on the decreased reaction rate and the increased influence of the C–C-scission side reaction.

In the previous studies such a dependency of the apparent activation energy on the cluster size has been explained by a difference in the activation energy on edges and terraces.[38] A similar explanation has served as a basis for theoretical development in ref.,[38] where explicit expressions for different reaction mechanisms have been derived, including the Langmuir-Hinshelwood mechanism of surface reaction kinetics. The latter implies quasi-equilibrium adsorption of two reactants and

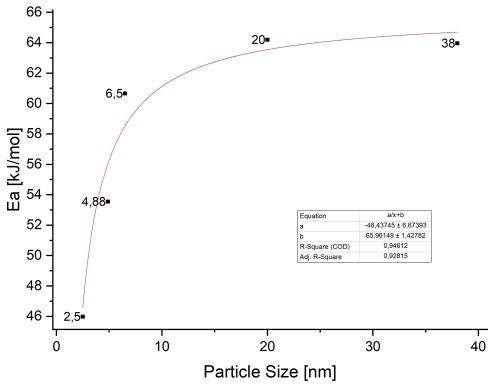

Figure 22. Dependence of activation energy on the nanoparticle size in oxidation of glucose with hydrogen peroxide: the line corresponds to Equation (2) and the squares to the experimental data.

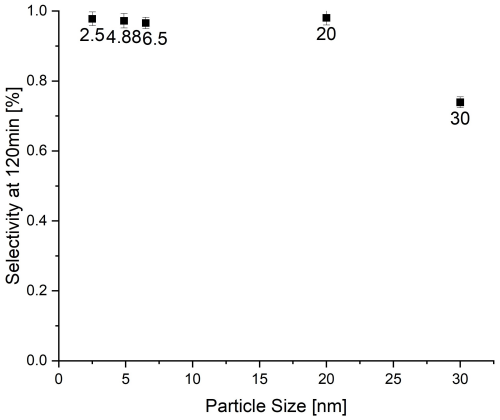

Figure 23. Dependence of selectivity to gluconic acid on the gold nanoparticle size.

their subsequent reaction on the surface. For the current case of glucose oxidation with hydrogen peroxide, the generic rate equation takes the form of Equation (2):

$$v = \frac{kC_{H_2O_2}C_{gluc}e^{\frac{-\alpha(\Delta\Delta G_{ads,H_2O_2}+\Delta\Delta G_{ads,gluc})/d_{cluster}-E_{reaction}-\Delta H_{H_2O_2}-\Delta H_{gluc}}{RT}}}{(1+K^{0,t}_{H_2O_2}C_{H_2O_2}e^{\frac{-\Delta G_{ads,H_2O_2}/d_{cluster}-\Delta H_{H_2O_2}}{RT}}+K^{0,t}_{gluc}C_{gluc}e^{\frac{-\Delta G_{ads,gluc}/d_{cluster}-\Delta H_{gluc}}{RT}})^2} \quad (2)$$

where k is a merged rate constant, $K^{0,t}_{H_2O_2}$ and $K^{0,t}_{gluc}$are adsorption coefficients for hydrogen peroxide and glucose on terraces, $\Delta\Delta G_{ads,H_2O_2} = (\Delta G_{ads,edges,H_2O_2} - \Delta G_{ads,terraces,H_2O_2})$ reflects the difference in the Gibbs adsorption energy of hydrogen peroxide and glucose on edges and terraces, $C_{H_2O_2}; C_{gluc}$and $\Delta H_{H_2O_2}; \Delta H_{gluc}$corresponds to the concentrations and the heats of adsorption of these molecules on terraces, $E_{reaction}$is the activation energy of the reaction between adsorbed hydrogen peroxide and glucose, α is the Polanyi parameter for the surface reaction and $d_{cluster}$is the cluster diameter.

Equation (2) can be essentially simplified for first order kinetics in both reactants, which is the case of glucose oxidation with hydrogen peroxide in the current study. The rate equation becomes Equation (3)

$$v = kC_{H_2O_2}C_{gluc}e^{\frac{-\alpha(\Delta\Delta G_{ads,H_2O_2}+\Delta\Delta G_{ads,gluc})/d_{cluster}-E_{reaction}-\Delta H_{H_2O_2}-\Delta H_{gluc}}{RT}} \quad (3)$$

The apparent activation energy for Equation (3) consists of following contributions [Equation (4)]:

$$E_{app} = \alpha(\Delta\Delta G_{ads,H_2O_2}+\Delta\Delta G_{ads,gluc})/d_{cluster} + E_{reaction} + \Delta H_{H_2O_2} + \Delta H_{gluc} \quad (4)$$

Fitting this model to the experimentally observed apparent activation energies resulted in a good description of the experimental data as shown in Figure 20 < xfigr20The analysis revealed a strong influence of the cluster size on the apparent activation energy which was related to substantial differences in the Gibbs adsorption energy on terraces and edges and subsequently, in the activation energy. The value of parameter $\alpha(\Delta\Delta G_{ads,H_2O_2}+\Delta\Delta G_{ads,gluc})$ was estimated to ca. -484 ± 6.6 kJ/mol, pointing out on a substantial difference between the Gibbs energy of adsorption of hydrogen peroxide and glucose on edges and terraces. The sum of $E_{reaction}+\Delta H_{H_2O_2}+\Delta H_{gluc}$ is ca. 66 ± 1.4 kJ/mol. It should be noticed that the structure sensitive behaviour of the activation energy has been demonstrated here for the first time for oxidation of glucose with hydrogen peroxide on gold catalysts.

Conclusions. The selective oxidation of glucose with hydrogen peroxide was studied using different supported gold, iron, palladium and tungsten catalysts. Gold catalysts displayed the highest gluconic acid yield exceeding 95 %. From the catalysts investigated, the alumina supported gold catalysts showed higher rates than the gold catalysts supported on titanosilicates. On the contrary, iron and palladium catalysts predominantly promoted C–C scission reactions leading to the production of mainly formic and levulinic acids. In the absence of an active metal, the supports catalysed C–C scission reactions with an autocatalytic behaviour in the formation of formic acid. For the first time, the structure sensitivity for this reaction was demonstrated on gold catalysts. The study revealed a rate maximum around 6.5 to 7 nm in the gold nanoparticles for the standard reaction conditions. Determination of the activation energies for the particle sizes uncovered a change in the apparent activation energy. A model for the change on activation energy based on the Langmuir-Hinshelwood type mechanism was applied, leading to a good description of the experimental data.

Experimental Section

Chemicals. For the catalyst synthesis $HAuCl_4$ (Alfa Aesar), $Fe(NO)_3$ (Sigma Aldrich) and $Pd(NO_3)_2$ (Alfa Aesar) as precursors and 30 % NH_3 solution (Merck) were used. The support γ-Al_2O_3 (UOP) and TS-1 (ACS-Materials) were used as supplied. The experiments were done using anhydrous D(+)-Glucose (Fluka), NaOH (Fischer Scientific) and 30 % H_2O_2 (Sigma Aldrich).

Catalyst synthesis and characterization. TiMWW was prepared according to the method of Wu et al.[14] The gold catalysts were synthesised by the deposition-precipitation (DP) method using ammonium hydroxide according to Bevaresh et al.[20] or the evaporation impregnation method (EI). To achieve the targeted gold nanoparticle sizes, the dosing policy and calcination temperature and the synthesis method were varied. For the DP, 4 g of the support were suspended in 500 ml ultrapure water and stirred vigorously for 3 h and heated to 70 °C. Afterwards a corresponding amount of gold precursor was added and the pH was raised stepwise to pH = 8 using 30 % ammonia solution. The pH was raised in different step sizes every 30 min with either 2 steps (pH = 6/pH = 8), 3 steps (pH = 4.5/pH = 6/pH = 8) or in one step (pH = 8) with an overall aging time of 3 h. After the aging the catalysts was filtered and washed with ultrapure water and dried overnight at 50 °C. In the evaporation impregnation method 4 g of the support a corresponding amount of gold precursor were dispersed in water and aged at 50 °C for 24 h and then dried under vacuum. All gold catalysts were then calcined using the method described by Bevaresh et al.[26] The Table 4gives an overview on the synthesis conditions of the gold catalysts. The tungsten and iron catalysts were prepared using incipient wetness impregnation (IW) with $W(NO_3)_6$ or $Fe(NO_3)_3$ respectively. For that 2 g of the support were

Table 4. Conditions for synthesis of gold catalysts.

Catalyst	Method	Addition of base	T_{calc} [°C]
2wt% Au/Al_2O_3 2.5 nm	DP	3 steps	300
2wt% Au/Al_2O_3 3 nm	DP	3 steps	300
2wt% Au/Al_2O_3 4.88 nm	DP	3 steps	500
2wt% Au/Al_2O_3 6.5 nm	DP	2 steps	300
2wt% Au/Al_2O_3 7 nm	DP	2 steps	300
2wt% Au/Al_2O_3 20 nm	DP	1 step	300
2wt% Au/Al_2O_3 38 nm	EI	no added base	300

mixed with a volume of a solution of ultrapure water and a corresponding amount of the precursor corresponding to the pore volume of the support. The catalysts were then dried overnight and calcined at 450 °C. The palladium catalyst was synthesized by evaporation impregnation. The metal loading of all the catalysts were targeted at 2 wt% metal loading with exception of the palladium based catalyst. The metal particle size distribution and the metal dispersion were determined with Transmission Electron Microscope (TEM) (JEM-1400 Plus TEM) and the metal loading with Scanning Electron Microscope with Energy Dispersive Spectroscopy (SEM-EDS), while the acidity was determined with NH_3-TPD (BellCat II).

Catalytic experiments. All experiments were carried out in an isothermal 250 ml glass reactor fitted with a Teflon stirrer depicted in Figure 24.

The pH of the system was controlled by a pH-controller (Metrohm) dosing 1 M NaOH and fixed at pH = 8. The temperature of the reactor jacket was maintained constant with a thermostat (Julabo).

For the kinetic experiments with hydrogen peroxide as the oxidant, an aqueous glucose solution was placed in the reactor and the system was heated to 30 °C, 70 °C, and 90 °C, respectively. Similarly to the reference experiments, the pH-control was started after reaching the desired temperature. The catalyst (100 mg) was added simultaneously with hydrogen peroxide. The ratio of hydrogen peroxide and glucose solutions were adjusted to reach the final concentrations of 0.75 M and 1.5 M of hydrogen peroxide and 0.2 M of glucose. The corresponding blank experiments were conducted in the absence of the catalyst, with the support materials and with hydrogen peroxide in the absence of glucose.

The samples were withdrawn from the reaction mixture at different reaction times. The organic components were analysed with HPLC (Agilent) using an Aminex HPX-87 C column (80 °C, 1.2 M $CaSO_4$, 0.6 ml/min) while the concentration of hydrogen peroxide was determined by ceric sulphate titration.

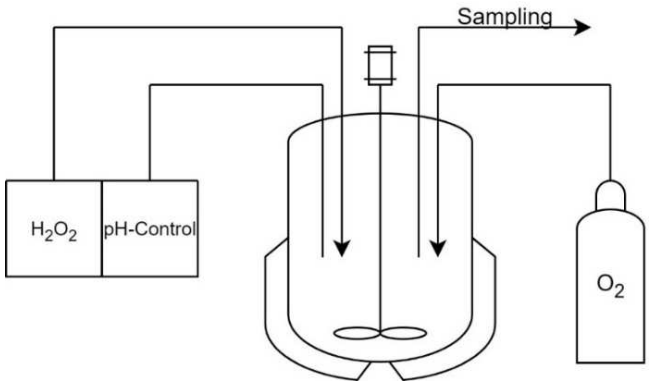

Figure 24. Set-up for catalyst screening and kinetic experiments.

Acknowledgements

This work is a part of the activities financed by Academy of Finland, through the Academy Professor grants 319002, 320115, 345053 (T. Salmi, O. Reinsdorf, M. Alvear). Financial support from Fortum and Neste Foundation (C. Schmidt) and the Erasmus program (C. Pellegrin) is gratefully acknowledged.

Conflict of Interests

The authors declare no conflict of interest.

Data Availability Statement

The data that support the findings of this study are available from the corresponding author upon reasonable request.

Keywords: gold catalysis · heterogeneous catalysis · hydrogen peroxide · structure sensitivity · sugar oxidation

[1] J. N. Chheda, G. W. Huber, J. A. Dumesic, *Angew. Chem. Int. Ed.* **2007**, *46*, 7164.
[2] C. Baatz, U. Prüße, *Catal. Today* **2007**, *122*, 325.
[3] T. Ishida, H. Watanabe, T. Bebeko, T. Akita, M. Haruta, *Appl. Catal. A* **2010**, *377*, 42.
[4] A. V. Tokarev, E. V. Murzina, K. Eränen, H. Markus, A. J. Plomp, J. H. Bitter, P. Mäki-Arvela, D. Y. Murzin, *Res. Chem. Interm.* **2009**, *35*, 155.
[5] S. Franz, N. D. Shcherban, I. Bezverkhyy, S. A. Sergiienko, I. L. Simakova, T. Salmi, D. Y. Murzin, *Res. Chem. Interm.* **2021**, *47*, 2573–2587.
[6] I. V. Delidovich, O. P. Taran, L. G. Matvienko, A. N. Simonov, I. L. Simakova, A. N. Bobrovskaya, V. N. Parmon, *Catal. Lett.* **2010**, *140*, 14–21.
[7] X. Liang, C.-J. Liu, P. Kuai, *Green Chem.* **2008**, *10*, 1318–1322.
[8] B. T. Kusema, B. C. Campo, O. A. Simakova, A. R. Leino, K. Kordas, P. Mäki-Arvela, T. Salmi, D. Y. Murzin, *ChemCatChem* **2011**, *3*, 1789.
[9] M. Haruta, *Catal. Today* **1997**, *36*, 153.
[10] S. Cattaneo, M. Strucchi, A. Villa, L. Prati, *ChemCatChem* **2019**, *11*, 309–323.
[11] W. Yan, D. Zhang, Y. Sun, Z. Zhou, Y. Du, Y. Du, Y. Li, M. Liu, Y. Zhang, J. Shen, X. Jin, *Chin. J. Catal.* **2020**, *41*, 1320–1336.
[12] H. Yan, M. Zhao, X. Feng, S. Zhao, X. Zhou, S. Li, M. Zha, F. Meng, X. Chen, Y. Liu, D. Chen, N. Yan, C. Yan, *Angew. Chem. Int. Ed.* **2022**, *61*, 134.
[13] H. Yan, S. Li, X. Feng, J. Lu, X. Zheng, R. Li, X. Zhou, X. Chen, Y. Liu, D. Chen, H. Shan, C. Yang, *AIChE J.* **2023**, *69*, 2.
[14] H. Yan, H. G. Qin, X. Feng, X. Jin, W. Liang, N. Sheng, C. Zhu, H. Wang, B. Yin, Y. Liu, X. Chen, C. Yang, *J. Catal.* **2019**, *370*, 434–446.
[15] T. Faverge, B. Gilles, A. Bonnefont, F. Maillard, C. Couyanceau, M. Chatanet, *ACS Catal.* **2023**, *13*, 2657–2669.
[16] M. Comotti, C. Della Pina, E. Falletta, M. Rossi, *Adv. Synth. Catal.* **2006**, *348*, 313–316.

[17] R. Saliger, N. Decker, U. Prüße, *Appl. Catal. B* **2011**, *102*, 584–589.
[18] M. Omri, F. Sauvag, Y. Busby, M. Becuwe, G. Pourceau, A. Wadouachi, *ACS Catal.* **2018**, *8*, 1635–1639.
[19] M. Omri, G. Pourceau, M. Becuwe, A. Wadouachi, *ACS Sustainable Chem. Eng.* **2016**, *4*, 2432–2438.
[20] P. Wu, T. Tatsumi, T. Komatsu, T. Yashima, *J. Phys. Chem. B* **2001**, *105*, 2897–905.
[21] S. Rautiainen, P. Lehtinen, M. Vehkamäki, K. Niemelä, M. Kemell, M. Heikkilä, T. Repo, *Catal. Commun.* **2016**, *74*, 115–118.
[22] U. Prüße, P. Jarzombek, K.-D. Vorlop, *Top. Catal.* **2012**, *55*, 453–459.
[23] J.-Y. Xin, K. Lin, Y. Wang, C.-G. Xia, *Int. J. Mol. Sci.* **2014**, *15*, 21603–21620.
[24] M. Wei, Y. Qiao, H. Zhao, J. Liang, T. Li, Y. Luo, S. Lu, X. Shi, W. Lu, X. Sun, *Chem. Commun.* **2020**, *56*, 14553.
[25] Y. Qiao, Q. Liu, S. Lu, G. Chen, S. Gao, W. Lu, X. Sun, *J. Mater. Chem. B* **2020**, *8*, 5411.
[26] E. Behravesh, N. Kumar, Q. Balme, J. Roine, J. Salonen, A. Schukarev, J.-P. Mikkola, M. Peurla, A. Aho, K. Eränen, D. Y. Murzin, T. Salmi, *J. Catal.* **2017**, *353*, 223–238.
[27] R. Turco, R. Tesser, V. Russo, T. Cogliano, M. Di Serio, E. Santacesaria, *Ind. Eng. Chem. Res.* **2021**, *46*, 16607–16618.
[28] M. Alvear, M. E. Fortunato, V. Russo, K. Eränen, M. Di Serio, J. Lehtonen, S. Rautiainen, D. Murzin, T. Salmi, *Ind. Eng. Chem. Res.* **2021**, *60*, 9429–9436.
[29] J. Prech, P. Eliásová, D. Aldhayan, M. Kubu, *Catal. Today* **2015**, *243*, 134–140.
[30] A. K. Sinha, S. Seelan, M. Okumura, T. Akita, S. Tsubota, M. Haruta, *J. Phys. Chem. B* **2005**, *109*, 3956–3965.
[31] F. Haber, J. Weiss, *Proc. R. Soc. Lond.* **1934**, *A147*, 332–351.
[32] S.-S. Lin, M. D. Gurol, *Environ. Sci. Technol.* **1998**, *32*, 1417–1423.
[33] A. L.-T. Pham, C. Lee, F. M. Doyle, D. L. Sedlak, *Environ. Sci. Technol.* **2009**, *43*, 8930–8935.
[34] F. Somma, G. Strukul, *J. Catal.* **2004**, *227*, 344–351.
[35] D. Prasetyoko, H. Fansuri, Z. Ramli, S. Endud, H. Nur, *Catal. Lett.* **2009**, *128*, 177–182.
[36] J. L. García-Gutiérrez, G. C. Laredo, P. García-Gutiérrez, F. Jiménez-Cruz, *Fuel* **2014**, *138*, 118–125.
[37] Y. Önal, S. Schimpf, P. Claus, *J. Catal.* **2004**, *223*, 122–133.
[38] D. Y. Murzin, *Catal. Lett.* **2019**, *149*, 1455–1463.

Manuscript received: April 19, 2023
Revised manuscript received: July 1, 2023
Accepted manuscript online: July 5, 2023
Version of record online: July 26, 2023